

Machinability of an Aluminium Cast Alloy Using PCD Tools for Turning

R.B. Soares, A.M.P. de Jesus, R.J.L. Neto, P.A.R. Rosa, M. Machado and A. Reis

1 Introduction

Aluminium–Silicon alloys are the most common cast alloys for the production of automotive components, especially for parts where the alloy is a substitute for cast iron. The high acceptance of these alloys is explained by the necessity of reducing the vehicles weight, without compromising the components strength. Besides that, these alloys present an excellent castability, low coefficient of thermal expansion, excellent wear-resistance and hot tearing resistance [1, 2].

Pure aluminium has adverse machinability characteristics, because the material tends to adhere to the rake and flank faces of the cutting tool, forming the so called built-up edges (BUE) [3]. The BUE formation deteriorates the surface quality of the component, the cutting stability and causes an accelerated tool wear. However,

R.B. Soares (✉) · A.M.P. de Jesus · R.J.L. Neto · M. Machado · A. Reis
INEGI, Faculdade de Engenharia, Universidade do Porto, Rua Dr. Roberto Frias, 400,
4200-465 Porto, Portugal
e-mail: rsoares@inegi.up.pt

A.M.P. de Jesus
e-mail: ajesus@fe.up.pt

R.J.L. Neto
e-mail: meto@inegi.up.pt

M. Machado
e-mail: mmachado@inegi.up.pt

A. Reis
e-mail: areis@inegi.up.pt

P.A.R. Rosa
IDMEC, Instituto Superior Técnico, Universidade de Lisboa, Av. Rovisco Pais, 1,
1049-001 Lisboa, Portugal
e-mail: pedro.rosa@tecnico.ulisboa.pt

when cutting speed increases or the application of cutting fluid is performed, the amount of adhered material layer can be reduced [3]. Another problem is the formation of long chips which are detrimental to their extraction from the cutting machine, disturb the surface finish of the produced parts and generally reduces the productivity of the machining operation. Although, the cutting forces and specific cutting pressures related to the machining of aluminium alloys are usually much lower, when compared to steel, with about 70% lower values [4].

In particular case of the hypoeutectic AlSi9Cu3 alloy, the microstructure consists of a dendritic α -Al solid solution and Al-Si eutectic, where Si assumes an acicular shape [5]. Due to the relatively high silicon content, around 9%, pronounced wear on cutting tools becomes a more relevant factor in the process. In addition, the presence of various impurities such as Fe and the presence of another alloying elements such Cu, lead to the appearance of complex intermetallic phases Fe-rich and Cu-rich. The eutectic Al₂Cu improve the machinability of the alloy because this constituent acts as a natural chip breaker and improve the quality of the machined surfaces. In other hand, the Fe-rich phases are harmful to both machinability and mechanical properties. The Al₅FeSi which precipitates in the interdendritic and intergranular regions, in the form of long and sharp needles, are strongly detrimental to the alloy mechanical properties including fatigue, but the presence of Mn reduces the formation of this phase and more complex Fe-rich phases can appear. These phases present a more compact morphology, in "chinese-script" or in polyhedral crystals (sludge), hard inclusions and also affects the tool life [6, 7].

These factors associated to the concept of high speed machining applied for the industries in order to increase the productivity, challenge the conventional sintered carbide tools, because the tool wear are excessive. For this reason, the turning of aluminium alloys, particularly the alloys with high content of Silicon, the maximum efficiency can be achieved with the use of polycrystalline diamond tools (PCD) or with the use of diamond coatings, applied to conventional carbide tools, by chemical vapour deposition (CVD). These inserts show low friction coefficient, high thermal conductivity, high-temperature hardness, chemical stability and abrasive wear resistance. These properties explain the high applicability of these tools in high speed machining of aluminium alloys [8, 9].

However, in the modern machining processes developed in automated machines, especially in turning operations, where continuous chips are commonly produced, the effective control of the type (shape and size) of the formed chips is fundamental. The formation of long chips difficult their right extraction from the working area, leads to production equipment stops and consequent loss of productivity, increases the tool wear and contributes to poor surface quality of the components [4, 10].

For the reasons above referred there is an increasing need to develop favourable conditions for the chip breaking without energy of cutting process and tool life factors being affected. One-way to overcome this challenge consists of using chip breakers, which are complex three-dimensional geometries in the tool rake face. The use of chip breakers in PCD tools is not yet a very common practice due to the difficulty of its production, which is an unfavourable point comparatively to Tungsten carbide inserts.

More than 75% of carbide inserts currently used by the industry have chip breaker structures which are produced with a very controllable cost.

During the recent years a great effort has been placed on chip control and chip breaking analysis, analytical models or FEM based software being often used to achieve a design methodology of these chip breakers [10–13]. But the complexity of the cutting phenomena associated to the complexity of grooved tools puts several limitations on predictive models and according to the industrial point of view, the chip control and the design of new complex three-dimensional chip breakers are normally based on try and see methodologies, supported by the strong experience from tool producers.

Another challenging is associated with the manufacture of the chip breaker structure in the rack face in the PCD inserts due to the machining difficulty of this material. This material can be machined by Electrical Discharging Machining (EDM), with reduced free form, or by laser micromachining [14]. Nowadays, with the laser micromachining it is possible to shape smooth and three-dimensional complex chip breakers in PCD inserts, with the needed accuracy and surface roughness.

In this study, an experimental evaluation of the PCD inserts with and without chip breakers was carried out in a specific aluminium alloy, used for automotive parts. Machining tests were performed in order to verify the performance of the cutting inserts and the influence of the chip breakers in the cutting forces, power consumption, specific cutting pressure, chip shape and size and surface roughness. For this propose, several cutting parameters are varied in external cylindrical turning operations.

2 Experimental Procedure

2.1 Material

The material selected for this study was the cast aluminium alloy specified as AISi9Cu3, according to the NP EN 1706 standard. The test samples for the machinability turning tests were obtained by permanent mould casting process. This casting process was performed in a coreless induction furnace at 730 °C. Hydrogen degassing was carried out with the use of an appropriated component based on Nitrogen (Nital C19) and the casting process was performed manually using a cooper permanent mould. This casting procedure aimed the provision of test cylinders of approximately 55 mm in diameter and 180 mm in length.

Table 1 compares the alloy chemical composition according to the NP EN 1706 standard and the composition of the alloy produced for this study, obtained by the spark spectrometry analysis. We realize that the chemical composition of the cast alloy is within the NP EN 1706 standard limits for the AISi9Cu3 aluminium alloy.

Table 1 Chemical composition of AlSi9Cu3 used in this study (element wt. %)

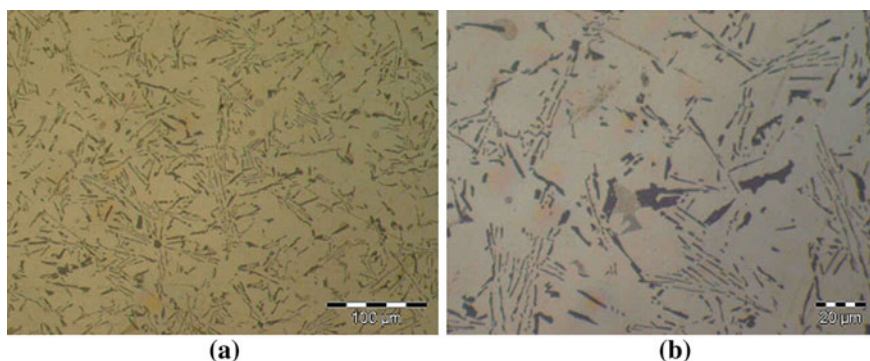
	Si	Fe	Cu	Mn	Mg	Ni	Pb	Ti	Al
NP EN 1706 standard AlSi9Cu3	8.0–11.0	1.3 max.	2.0–4.0	0.55 max.	0.05–0.55	0.55 max.	0.35 max.	0.25 max.	Remaining
Alloy used in this study	9.88	0.159	3.35	0.012	0.139	0.005	0.018	0.062	

After casting process, a sample for microstructural analysis was cut from a machining test sample. This material sample was polished by a standard metallographic procedure. An Olympus PMG3 optical microscope was used for the metallographic examination across the transversal section of the machining test samples. After the microstructural analysis, the same sample was submitted to a Brinell hardness test, in three distinct zones, across the transversal section of the machining test specimens. For this purpose a hardness machine Emco M4U-075 was used. The hardness test results are represented in the Table 2.

Figures 1 and 2 show the microstructures of the alloy used in the experimental study. By comparison with other analyses in the literature [5, 15], it can be verified

Table 2 Mechanical properties of AlSi9Cu3 used in this experimental study (average values of various tests)

Young's modulus (GPa)	66
Ultimate tensile strength (MPa)	196
Yield tensile strength (MPa)	91
Tensile elongation at failure (%)	3.2
Ultimate compressive strength (MPa)	524
Yield compressive strength (MPa)	199
Compressive elongation at failure (%)	30
Brinell hardness (HB)	87

**Fig. 1** Microstructure of AlSi9Cu3 alloy used in this study: **a** α -Al solid solution and Al-Si eutectic, Si in acicular shape; **b** presence of Cu-rich and Fe-rich phases

the dendritic α -Al solid solution and Al-Si eutectic, where Si assumes an acicular shape. Furthermore, it can be seen the presence of Fe-rich phase in polyhedral crystals and the presence of eutectic Al_2Cu (Fig. 1b). The presence of porosity (Fig. 2) confined to the central zone of the test samples, resultant of the casting and cooling process, did not influence the machining test results since a minimum diameter of 25 mm was not machined from the casted rods.

In addition to the previous material characterization, mechanical properties were evaluated from monotonic tensile tests in accordance with the EN 10002 standard and compression tests using cylindrical specimens, according to the ASTM E 9-89a standard. Figures 3 and 4 illustrate the resulting engineering stress-strain curves from both tensile and compressive tests respectively. Table 2 summarizes the mechanical properties extracted from the tensile tests. It can be observed that this material presents significantly different tensile and compressive strength behaviours. The tensile behaviour of this material is significantly less ductile than the

Fig. 2 Microstructural analysis in central zone of machining test pieces with some porosity

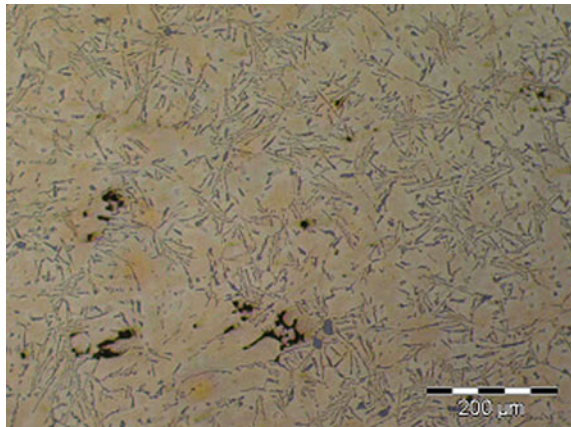


Fig. 3 Stress-strain curves from tensile tests

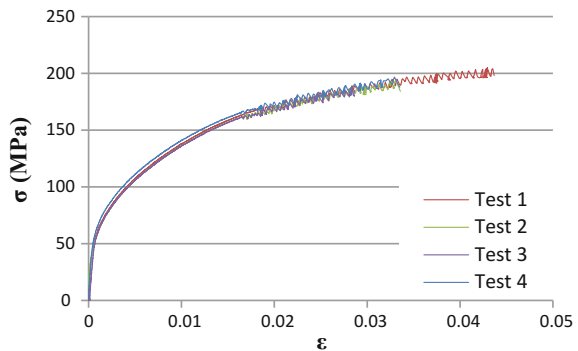
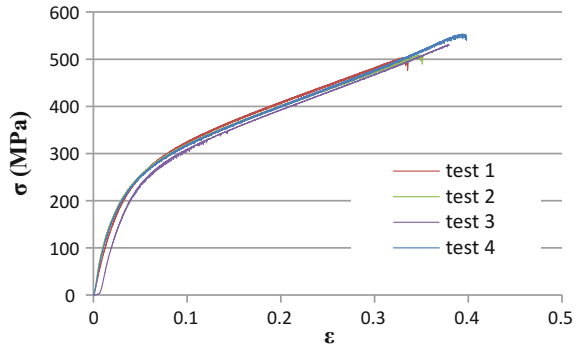


Fig. 4 Stress-strain curves from compressive tests



compressive behaviour as confirmed by the very distinct elongations. Also the strength values under tension are significantly lower than corresponding values under compression.

2.2 Machinability Tests

Machinability tests are evaluated using different solutions of commercially available cutting inserts proposed for the turning of aluminium alloys. Three different PCD tools were selected from Mapal tools manufacturer, one without chip breaker and two with different chip breaker geometries, CB1 and CB2 geometries. The CB1 geometry is indicated for finishing operations and the CB2 geometry is suggested for roughing operations. Figure 5 shows the PCD inserts and the designation of these inserts, according to the ISO 1832 standard. The same tool holder, with the specification SDJCL 2020 K11 was used in all cutting tests. The Table 3 presents the geometrical details of cutting inserts and tool holder.

A set of machining tests was performed in a EFI DU20 conventional horizontal lathe with 5.9 kW spindle power and a maximum spindle speed of 2500 rpm. These

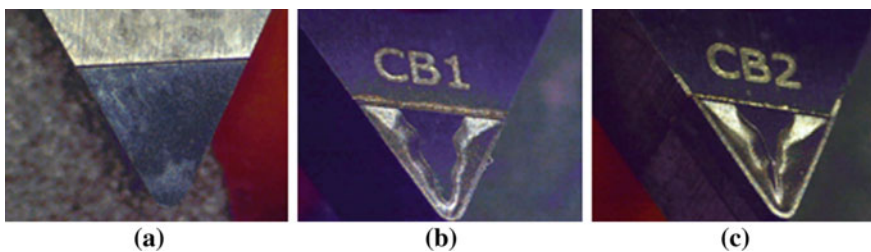


Fig. 5 PCD cutting inserts used in the machining tests: **a** flat rake face tool, DCGW 11T304 F01N-0AA; **b** CB1 geometry, DCGT 11T304 F01N-C1A; **c** CB2 geometry, DCGT 11T304 F01N-C2A

tests were instrumented in order to measure the cutting force components such as main cutting force (F_c), the feed force (F_f) and the passive force (F_p). A Kistler piezoelectric three-component dynamometer type 9257B, with a charge amplifier Kistler 5007 and a HBM Spider 8 acquisition system were used to acquire the signals of the cutting forces. The signals coming from dynamometer were evaluated using the *Catman* Software. Figure 6 illustrates the experimental setup concerning the turning tests on the conventional lathe.

The cutting parameters selected for the machining tests performed in the conventional lathe were defined based on the producer of the PCD inserts and also taking into account the limitations of the machine. Two spindle speeds were selected, namely 2500 and 900 rpm, with three cutting depths in the range of 0.25–1.5 mm and three feed rates in the 0.05–0.25 mm range. These cutting conditions are summarized in the Table 4.

Since the conventional lathe does not allow a constant cutting speed, the same machining sequence (a_p , f) was fully respected for each cutting insert, in order to allow a direct comparison of the result, which is generated for the same cutting velocities even they are varying with the diameter reduction. For the spindle speed of 2500 rpm resulted cutting speeds in the range of 350–432 m/min; for the spindle speed of 900 rpm resulted cutting speeds in the range of 88–117 m/min.

Table 3 Geometrical details of the inserts and tool holder used in machining tests

Insert shape (rhombic)	55°
Nose radius (r_ϵ)	0.4 mm
Clearance angle (α)	7°
Rake angle (λ_o)	0°
Inclination angle (λ_s)	0°
Position angle (χ)	93°

Fig. 6 Experimental setup for measurement of cutting forces and surface roughness

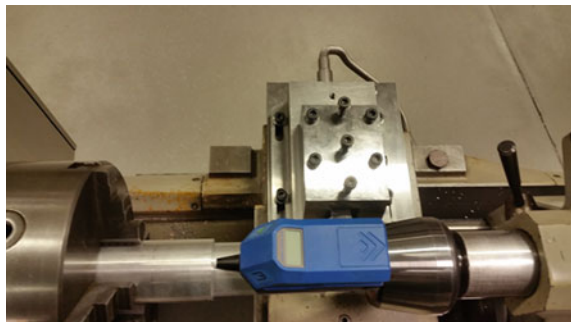


Table 4 Cutting parameters applied in cutting tests performed in the conventional lathe

Spindle speed (rpm)	2500; 900
Depth of cut (a_p) [mm]	0.25; 0.5; 1.5
Feed rate (f) [mm/rev]	0.05; 0.14; 0.25

Besides the cutting forces measurements, the chip typology and surface roughness were also evaluated during the machinability tests. For each turning test, chip samples are collected for the implementation of comparative tables. This procedure consists in organizing the chips corresponding to cutting parameters used in tests, in order to compare the different sizes and shapes and classify it according to the standard ISO 3685. Concerning the surface roughness measurements, three different zones of samples (cylinder), were assessed. This was performed according longitudinal lines equally spaced by 120° . This procedure allows the evaluation of the average roughness (R_a) and maximum height of roughness profile (R_{max}). The portable surface roughness tester Hommel Tester T500 was used for this analysis.

Once the conventional lathe machine used in this investigation only show a maximum modest spindle speed to the purpose of machinability tests with PCD inserts, additional tests were performed in a CNC GILDEMEISTER CXT400 lathe. This machine has a 36 kW spindle power and a maximum spindle speed of 5000 rpm, therefore, this machine permits the execution of machining tests with a maximum cutting speed of 690 m/min for the specimens diameters considered in the study. In addition to this cutting speed of 690 m/min, a smaller cutting speed of 300 m/min was used, and the same cutting depths and feed rates from Table 4 were applied again. These tests were performed under constant cutting speed. Only chip geometry and surface roughness's were evaluated in the tests performed in the CNC turning machine since the available load cells are not compatible with this machine.

3 Results and Discussion

3.1 Influence of Cutting Inserts and Cutting Parameters on Cutting Forces

Figures 7 and 8 illustrates typical cutting forces components, particularly the main cutting force (F_c), the feed force (F_f) and the passive force (F_p), along the machining time, for two different turning tests. In these specific cases, the insert used is the flat

Fig. 7 Example of cutting forces components for insert without chip breaker.

($v_c = 424$ m/min,
 $a_p = 1.5$ mm/min,
 $f = 0.05$ mm/rot)

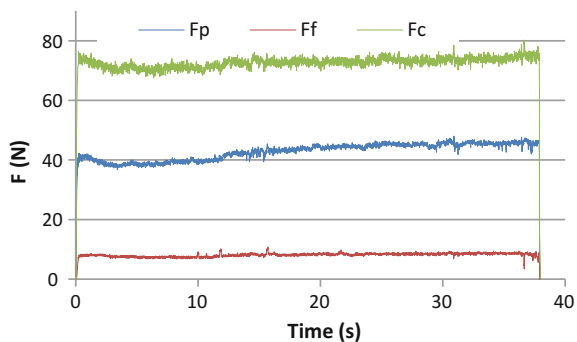
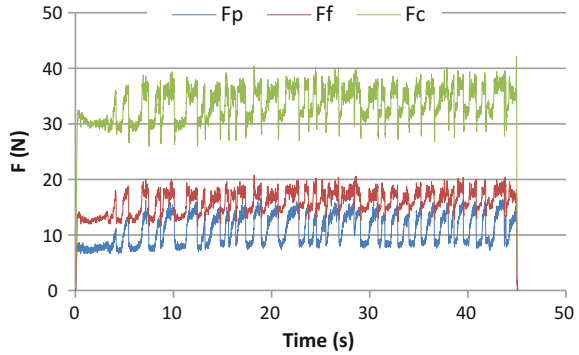


Fig. 8 Example of cutting forces components for insert without chip breaker ($v_c = 116$ m/min; $a_p = 0.25$ mm; $f = 0.14$ mm/rot)—influence of the BUE in cutting forces



rake face tool and the major difference between these results is the cutting speed. For low cutting speeds (Fig. 8) the results show an oscillatory evolution of cutting force consistent with the BUE phenomena.

Figure 9 shows the results of the average of the main cutting force (F_c), obtained for the cutting parameters considered in the conventional lathe, for two spindle speeds applied in the tests. Results show that the main cutting forces increase with increasing cutting depth and feed rate. In fact, the increase of these parameters results in increasing chip section and consequently the shear force required to deform the chip also increases. On the other hand, the increase of the cutting speed produces an opposite effect, which can be justified with a temperature increase of the material, which leads to a softening of the material and consequently lower deformation resistance is observed. In addition, for lower cutting speeds the BUE phenomenon becomes more apparent and this fact leads to a greater friction between the tool and the workpiece, which justifies higher cutting forces.

Comparing the main cutting forces obtained for each tested cutting insert, it is possible to verify that the flat face tool typically has lower cutting forces

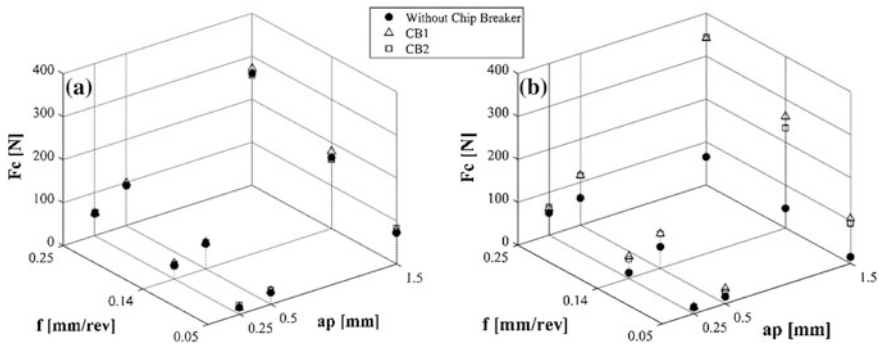


Fig. 9 Main cutting force variation with the feed rate and depth of cut for spindle speeds of 2500 rpm (a) and 900 rpm (b)

comparatively to inserts with chip breaker geometries present on the rake face. These results show that the presence of a groove in the rake face significantly increases the cutting forces which can be explained by the resistance to the natural flow of the chip generating higher cutting forces, as well as the increased frictional forces. Nevertheless, the forces generated in the cutting process are not dramatically influenced by the chip breaker geometries when high cutting speeds are considered.

3.2 Influence of the Inserts and Cutting Parameters on Cutting Power

Figure 10 shows the cutting power (P_c) as a function of the feed rate (f) and depth of cut (a_p), for each spindle speed used in the conventional lathe. The cutting power was calculated using the following equation, neglecting the cutting power generated by the feed movement:

$$P_c = v_c F_c \quad (1)$$

where F_c is the main cutting force, in N and v_c is the cutting speed in m/s.

The results concerning the cutting power show that the effect of different geometries of chip breakers do not have a significant influence in terms of energy required for the cutting process, in the case of the higher cutting speeds. Although the flat rake face insert is more advantageous from the energy consumption point of view, particularly for reduced f and a_p .

Another important observation is related to the cutting power evolution for the lowest range of tested cutting speeds, when the BUE phenomenon becomes quite evident. In this case, it appears that cutting power is much lower in flat rake face tool, revealing that the adhesion of the material is much lower in this type of tool,

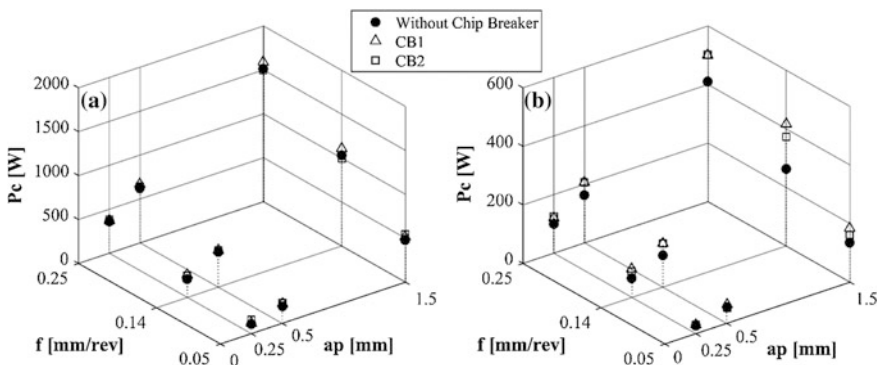
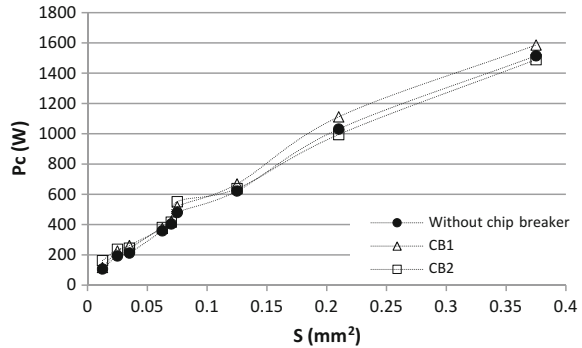


Fig. 10 Variation of cutting power with feed rate and depth of cut, for spindle speeds of 2500 rpm (a) and 900 rpm (b)

Fig. 11 Cutting power evolution as a function of the undeformed chip section (S) for 2500 rpm



and the groove in the rake face difficulties the evacuation of the adhered chips being a detrimental effect concerning the tool life.

Figure 11 represents the cutting power as a function of the undeformed chip section, for the spindle speed equal to 2500 rpm. In turning, the undeformed chip section (S), expressed in mm², is the product between the feed rate, in mm/rot and depth of cut, in mm. The analysis of the figure reveals the existence of some peaks or an oscillatory behaviour that are explained by the different contributions of the depth of cut and feed to the main cutting force values. In other words, for the increasing of the undeformed chip section the depth of cut and feed rate have different contributions in power consumption. For chip sections higher than 0.20 mm² can be observed that the use of the CB2 chip breaker geometry leads to substantially lower cutting power compared to the other inserts. This fact proves that obstacles to the chip flow can be produced still yielding an efficient chip control, with advantages in terms of energy consumption and also in terms of durability of the cutting tools.

3.3 Influence of the Inserts and Cutting Parameters on the Specific Cutting Pressure

The specific cutting pressure (K_s) was calculated using the following equation:

$$K_s = \frac{F_c}{S} \tag{2}$$

where F_c is the cutting force in N, and S the undeformed chip section in mm².

Figure 12 plots the specific cutting pressure K_s as a function of the feed and the cutting depth, for two different spindle speeds. It is clear the reduction of the specific cutting pressure when cutting depth or feed rate increases and the tendency to assume constant values for high values of these parameters. Another aspect is the influence of the cutting speed. For low cutting speeds it can be observed in some

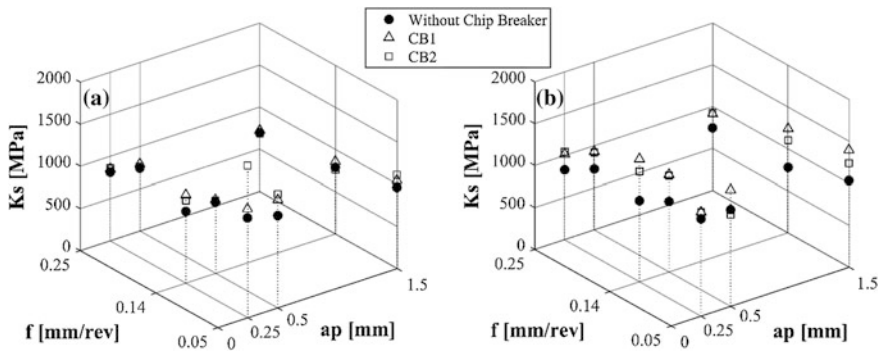
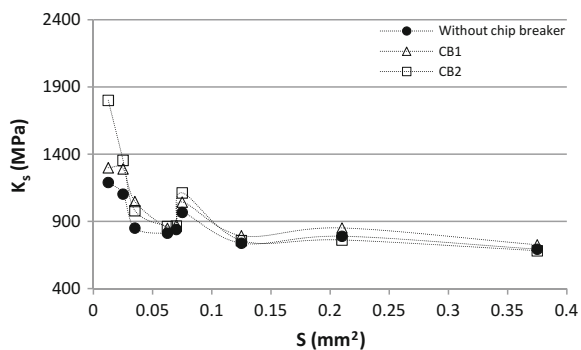


Fig. 12 Variation of specific cutting pressure (K_s) with feed rate and depth of cut for spindle speeds of 2500 rpm (a) and 900 rpm (b)

cases the increase of the K_s value. For these tested conditions it is notorious the effect of BUE formation, especially for inserts with chip breakers, where this phenomenon assumes a greater relevance and in some cases, produces a higher specific cutting pressure differently of what would be expected. Considering the higher cutting speeds, it can be concluded that all inserts presents similar K_s values under the same cutting conditions.

Figure 13 shows the evolution of the specific cutting pressure (K_s) with the undeformed chip section (S). From the figure it can be seen that the specific cutting pressure decreases with the increase of the chip section. In fact, it can be realized a size effect in the results obtained. For the lower chip sections, the friction effects between the tool and the chip, as well as the radius of the cutting tool tip can be an explanation for these results. For the higher tested undeformed chip section (0.38 mm^2), K_s values are in the range of $682\text{--}726 \text{ N/mm}^2$. These K_s values can be used as reference values for the industrial application, in particular for the estimation of the cutting forces.

Fig. 13 Comparison of specific cutting pressure with undeformed chip section (S) for spindle speeds of 2500 rpm



3.4 Influence of Cutting Inserts on Chip Morphology

Chip control (shape and size) is an aspect extremely important in turning operations, especially in case of ductile material, such aluminium alloys, machined with high cutting speed in automated machines. Effective control of the shape and size of the chips generated by the cutting process allows high levels of productivity and surface quality of the components.

Thus, for each machining test, chip samples were extracted, in order to allow a comparison between the inserts and to verify the effectiveness of the chip breakers for different cutting conditions. During some tests, especially for the flat face insert and the insert with CB2 chip breaker geometry applied in finishing conditions, long chips (e.g. ribbon chips) were obtained, which are harmful to the cutting process. The Tables 5 and 6 shows the comparison of the chips obtained for each insert. For the feed rate equal to 0.05 mm/rev we can observe that CB1 geometry is the only one that produced short chips (see Table 5). These results indicate that, this geometry is best suited for finishing operations, from the point of view of chip control. On the other hand, for the feed rate of 0.14 mm/rev the chip breaker CB2 presents a good chip control in these conditions while the flat face tool presents long chips and CB1 presents extremely short chips, producing higher cutting forces and power consumption, as previously seen. These results are represented in Table 6 and can be concluded that CB2 geometry works better for roughing operations.

For low cutting speed, in the range of 100–300 m/min, the execution of machining tests without cutting fluid causes the formation of BUE. The BUE formation results in short chips with a morphology revealing cutting instability (see

Table 5 Chip samples obtained for finishing operations ($f = 0.05$ mm/rev, $v_c = 690$ m/min)









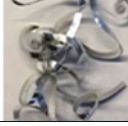









a_p (mm)	Without Chip Breaker	CB1 Geometry	CB2 Geometry
0.25			
0.5			
1.5			

Table 6 Chip samples obtained for semi-roughing operations ($f = 0.14 \text{ mm/rev}$, $v_c = 690 \text{ m/min}$)

$a_p(\text{mm})$	Without Chip Breaker	CB1 Geometry	CB2 Geometry
0.25			
0.5			
1.5			

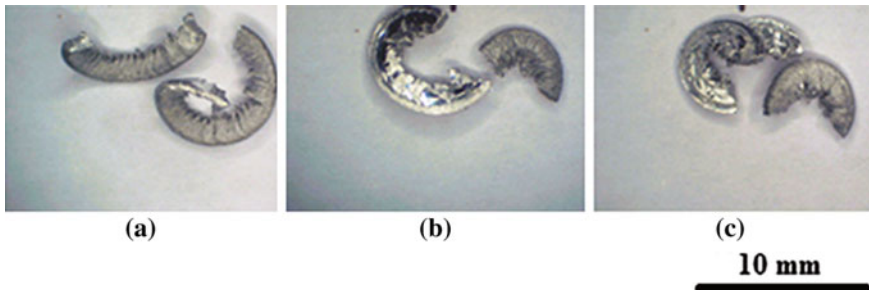


Fig. 14 Example of the effect of BUE formation in chip morphology for each insert used: **a** Without chip breaker; **b** CB1 geometry; **c** CB2 geometry

Fig. 14). This fact results in worse surface roughness, verified in the next section, and affects the tool life.

3.5 Influence of Cutting Inserts on Surface Roughness

Another important parameter in the evaluation of the machinability, depending of tool used, is related to the surface quality of the workpiece. Often, the surface quality is interpreted by the surface roughness of machined components. Therefore the average roughness or just roughness (R_a) and maximum height of roughness profile (R_{max}) were evaluated for each surface resulting from the machining tests.

For comparison purposes, experimental roughness results are compared with theoretical values represented by R_{at} and R_{maxt} and given by the following equations:

$$R_a = \frac{f^2}{32 r_e} \times 1000 \tag{3}$$

$$R_{tmax} = \frac{f^2}{8 r_e} \times 1000 \tag{4}$$

where f is the feed rate in mm/rev, and r_e the nose radius of the insert in mm.

The quality of the machined surface is dependent of the cutting conditions selected for each test. In fact, the surface roughness it is more dependent of the cutting conditions and insert nose radius than the different type of inserts. The feed rate is the parameter that shows the higher influence in surface roughness, an increase in feed rate affecting negatively the surface quality (Fig. 15). Therefore, low feed rates are implemented in finishing machining.

Figures 16 and 17 show the influence of the cutting speed on the surface roughness. It can be concluded that the value of R_a decreases with the cutting speed. This aspect is directly associated to the BUE formation. For cutting speeds lower

Fig. 15 Surface roughness (R_a) function of the feed rate ($a_p = 0.25$ mm; $v_c = 690$ m/min)

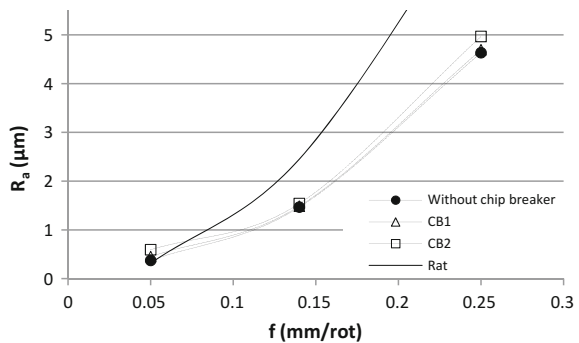


Fig. 16 Surface roughness (R_a) function of the cutting speed ($a_p = 0.25$ mm; $f = 0.05$ mm/rot)

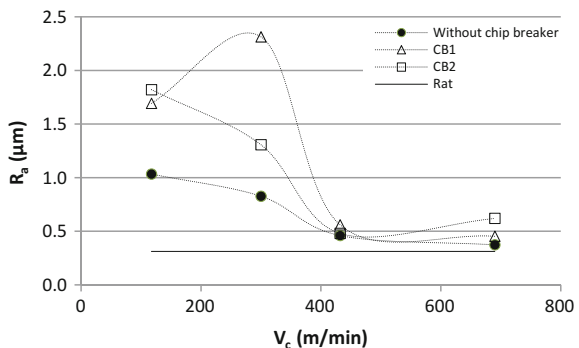


Fig. 17 Surface roughness (R_a) function of the cutting speed ($a_p = 0.5$ mm; $f = 0.05$ mm/rot)

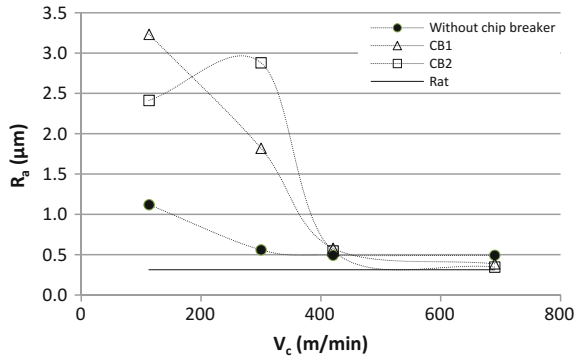
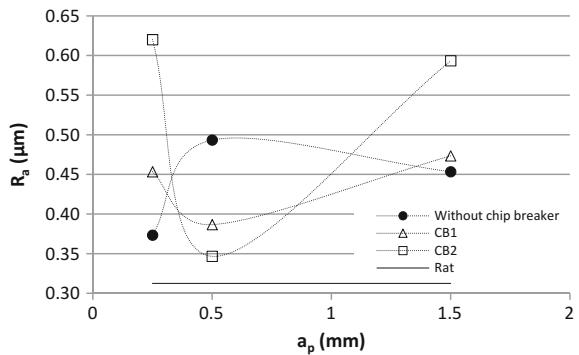


Fig. 18 Surface roughness (R_a) function of the cutting depth (a_p) ($f = 0.05$ mm/rot and $v_c = 690$ m/min)



than 300 m/min the surface roughness increases quickly. The adhesion of the material to the cutting tool edge as well as to new machined surfaces compromises the surface quality of the component. Although, in the flat rake face tool the adhesion of the material is less evident, consequently the influence in R_a value is less significant. Therefore, the flat face insert is the more indicated tool for low cutting speeds especially, in the case of dry machining.

The depth of cut also influences the surface roughness, this influence depending on cutting insert used. Figure 18 confirms that exist an optimal cutting depth for each insert to improve surface quality. The flat rake face tool presents the better results for R_a for depth of cut equal to 0.25 mm, whereas the inserts with chip breakers present the best results for depths of cut equal to 0.5 mm.

4 Conclusions

The influence of the chip breaker geometries and the cutting parameters (cutting speed, depth and feed rate) on machinability of the AlSi9Cu3 cast alloy were experimentally investigated and the following conclusions could be draw:

- The results showed a tendency to built-up edge formation for low cutting speeds for all of the inserts tested and this fact is responsible for higher cutting forces, power consumption and it also disturbs surface quality. However, this tendency of BUE formation can be reduced by the use of flat face tools;
- For chip sections higher than 0.20 mm^2 the use of the CB2 chip breaker geometry led to substantially lower cutting power, compared to the others inserts associated to efficient chip control, for this conditions;
- Regarding the specific cutting pressure values, it is notorious the size effect for lower undeformed chip sections, but in the case of higher undeformed chip sections the values the specific cutting pressure tends constant values. Considering the higher undeformed chip section tested (0.38 mm^2), K_s presents values in the range of $682\text{--}726 \text{ N/mm}^2$, for CB2 and CB1 chip breaker geometries respectively;
- The use of flat face inserts generates long chips for the majority of applied cutting conditions. On the other hand, the CB1 geometry presents an efficient chip control for low feed rates (0.05 mm/rev). This chip breaker is suitable for finishing operations, but this insert leads to higher power consumption. On the other side, the CB2 geometry presents an effective chip control for feed rates in the order of 0.14 mm/rev , and still presents, for these parameters, lower specific pressures values and lower cutting power;
- The surface roughness increases with the feed rate, but for feed rates equal to 0.05 mm/rev , there exists an optimum cutting depth. It can be possible to obtain surface roughness in the order of $0.35 \text{ }\mu\text{m}$ for CB2 geometry, $0.37 \text{ }\mu\text{m}$ for the flat face tool and $0.39 \text{ }\mu\text{m}$ for the CB1 geometry.

Acknowledgements Authors acknowledge the funding of Project NORTE-01-0145-FEDER-000022—SciTech, co-financed by NORTE2020, through FEDER. Authors also acknowledge MAPAL Company which offered the cutting inserts.

References

1. Tanaka, T., Akasawa, T.: Machinability of hypereutectic silicon-aluminum alloys. *J. Mater. Eng. Perform.* **8**, 463–468 (1999)
2. Timelli, G., Fabrizi, A.: The effects of microstructure heterogeneities and casting defects on the mechanical properties of high-pressure die-cast AlSi9Cu3(Fe) alloys. *Metall. Mater. Trans. A-Phys. Metall. Mater. Sci.* **45**, 5486–5498 (2014)
3. Sood, P.K., Sehgal, R., Dwivedi, D.K.: Machinability study of stir cast hypoeutectic aluminum-silicon alloys during turning. *J. Mater. Eng. Perform.* **22**, 470–482 (2013)
4. Santos, M.C., Machado, A.R., Sales, W.F., Barrozo, M.A.S., Ezugwu, E.O.: Machining of aluminum alloys: a review. *Int. J. Adv. Manuf. Technol.* 1–14 (2016)
5. Puga, H., Costa, S., Barbosa, J., Ribeiro, S., Prokic, M.: Influence of ultrasonic melt treatment on microstructure and mechanical properties of AlSi9Cu3 alloy. *J. Mater. Process. Technol.* **211**, 1729–1735 (2011)

6. Ferraro, S., Timelli, G.: Influence of sludge particles on the tensile properties of die-cast secondary aluminum alloys. *Metall. Mater. Trans. B-Proc. Metall. Mater. Proc. Sci.* **46**, 1022–1034 (2015)
7. Davis, J.R.: *Aluminum and aluminum alloys*. ASM International, Materials Park, OH (1993)
8. Basavakumar, K.G., Mukunda, P.G., Chakraborty, M.: Influence of melt treatments and turning inserts on cutting force and surface integrity in turning of Al-12Si and Al-12Si-3Cu cast alloys. *Surf. Coat. Technol.* **201**, 4757–4766 (2007)
9. Kalyan, C., Samuel, G.L.: Cutting mode analysis in high speed finish turning of AlMgSi alloy using edge chamfered PCD tools. *J. Mater. Process. Technol.* **216**, 146–159 (2015)
10. Gonzalo, O., Quintana, I., Etxarri, J.: FEM based design of a chip breaker for the machining with PCD tools. *Adv. Mater. Res.* **223**, 133–141 (2011)
11. Shinozuka, J., Obikawa, T., Shirakashi, T.: Chip breaking analysis from the viewpoint of the optimum cutting tool geometry design. *J. Mater. Process. Technol.* **62**, 345–351 (1996)
12. Kim, H.G., Sim, J.H., Kweon, H.J.: Performance evaluation of chip breaker utilizing neural network. *J. Mater. Process. Technol.* **209**, 647–656 (2009)
13. Jawahir, I.S., Fang, X.D.: A knowledge-based approach for designing effective grooved chip breakers—2D and 3D chip flow, chip curl and chip breaking. *Int. J. Adv. Manuf. Technol.* **10**, 225–239 (1995)
14. Miyazawa, H., Takeuchi, S., Miyake, S., Murakawa, M.: Sintered diamond cutting inserts with chip breaker prepared by laser technique. *Surf. Coat. Technol.* **86–87**, 797–802 (1996)
15. Panušková, M., Tillová, E., Chalupová, M.: Relation between mechanical properties and microstructure of cast aluminum alloy AlSi9Cu3. *Strength Mater-Engl. Tr.* **40**, 98–101 (2008)